M5AIE
A Method for Body Part Detection and Tracking using RGB-D Images

André Brandão[1,2], Leandro A. F. Fernandes[1] and Esteban Clua[1]

[1]*MediaLab-UFF, Instituto de Computação, Universidade Federal Fluminense, CEP 24210-240 Niterói, RJ, Brazil*

[2]*German Research Center for Artificial Intelligence (DFKI GmbH), Kaiserslautern, Germany*

Keywords: Body-part Detection, Tracking, Pose Classification, AGEX, ASIFT, Depth Images, Medial Axis.

Abstract: The automatic detection and tracking of human body parts in color images is highly sensitive to appearance features such as illumination, skin color and clothes. As a result, the use of depth images has been shown to be an attractive alternative over color images due to its invariance to lighting conditions. However, body part detection and tracking is still a challenging problem, mainly because the shape and depth of the imaged body can change depending on the perspective. We present a hybrid approach, called M5AIE, that uses both color and depth information to perform body part detection, tracking and pose classification. We have developed a modified Accumulative Geodesic Extrema (AGEX) approach for detecting body part candidates. We also have used the Affine-SIFT (ASIFT) algorithm for feature extraction, and we have adapted the conventional matching method to perform tracking and labeling of body parts in a sequence of images that has color and depth information. The results produced by our tracking system were used with the C4.5 Gain Ratio Decision Tree, the Naïve Bayes and the KNN classification algorithms for the identification of the users pose.

1 INTRODUCTION

Human body part detection, tracking and pose classification are challenging tasks because a humans shape varies from one person to another. Humans have different skin colors; their clothes can also vary in both color and shape, and movement patterns can differ from person to person. Reliable results on body part detection and tracking have been achieved by using depth images that were captured by specific sensors for this purpose. Depth images outperform intensity images in the sense that they intrinsically remove appearance features such as the color of imaged objects (Plagemann et al., 2010). Additionally, depth images provide extra information about the scene, such as the actual geometry of the objects. RGB information is also used for detecting and tracking human body parts, but the combination of RGB and depth information can be a powerful tool in this context.

RGB and depth images captured from the real world contain a large amount of information. Much of this information is irrelevant to human body part detection and pose recognition. Therefore, filtering the data is an important task, to reduce the computational load of the body part detection. Another issue in this context is how to track the body parts in a video sequence. Knowledge about each body part position yields information on pose recognition.

We present a method for performing data filtering, body part detection and tracking, and pose recognition. In our algorithm (see Fig.1), we first take the independent RGB pixels and depth information of a frame and produce an RGB-D image. Next, we filter the information using a background subtraction approach that is applied to the depth values, which reduces the image to foreground information only. In our case, the foreground is a person. To reduce even more the amount of data that is used in the pose estimation, we apply a medial axis transformation to the segmented image. The output of this stage will then be used to detect and label human body parts. With the labeled body parts in hand, it is possible to track each of them in the video sequence and to estimate the positions of the body parts according to their velocity.

Human pose classification is made for each frame using two different algorithms: the C4.5 Gain Ratio Decision Tree (Quinlan, 1993) and the Naïve Bayes Classifier (Domingos and Pazzani, 1997). In our approach, the input information for the classification stage is a set of 2D coordinates of the cells that contain the tracked body parts of the subject. The size and location of the cells is defined by a regular subdivision strategy that is applied on the RGB-D image.

The name M5AIE is an acronym for each of the

Brandao A., Fernandes L. and Clua E..
M5AIE - A Method for Body Part Detection and Tracking using RGB-D Images.
DOI: 10.5220/0004738003670377
In *Proceedings of the 9th International Conference on Computer Vision Theory and Applications* (VISAPP-2014), pages 367-377
ISBN: 978-989-758-003-1

used concepts in our approach: *M*edial *A*xis transformation, for data filtering; *A*dapted *A*GEX, for the body part detection; *A*SIFT, for the body parts tracking, *A*ligned *I*mages (RGB-D), and *E*stimation, also for tracking.

The main contributions of this paper include the following:

- The combination of AGEX and ASIFT methods using aligned RGB and depth images for labeling five major defined body parts (hands, feet and head); and
- Track each of the body parts using an adapted ASIFT matching algorithm.

This paper is organized as follows: Section 2 presents some of the related studies. Section 3 describes the M5AIE method. The results are presented in Section 4. Section 5 concludes the work with a discussion and future directions for the research.

2 RELATED WORK

Human action recognition is a related area of Computer Vision that addresses motion in videos. Mota et al. (Mota et al., 2012) introduced a video motion indexing scheme that was based on modeling optical flow. In their work, the authors proposed a global motion tensor descriptor for video sequences, and optical flow was described with a polynomial representation. In contrast to Mota et al.'s work, we are concerned with the detection and tracking of body parts in RGB-D image sequences and with pose identification in single frames of the sequence.

Several Computer Vision studies have solved movement recognition problems using either RGB or depth images. If we consider both RGB and depth values captured by a specific sensor and combine them, the possibility of correctly handling pose-recognition issues increases. In our work, we use depth information for background subtraction. The RGB information is used to produce RGB-D images that are converted to grayscale by the tracking method.

Regarding human pose recognition, Shotton et al. (Shotton et al., 2011) have described an approach that is based on single depth images captured with a Microsoft Kinect sensor. The main contribution of Shotton's work is to treat pose estimation as object recognition, using an intermediate body parts representation to find the joints with high accuracy.

An accurate pose estimator from single-depth images was described by Ye et al. (Ye et al., 2011). These authors used a dataset as input to make the pose estimation and presented a pose refinement scheme that can handle pose and body size differences. In their work, they also proposed a pose detection algorithm that is view independent.

A combination of RGB and depth images (RGB-D) has been used for different purposes. Henry et al. (Henry et al., 2012) presented how the RGB-D images can be used to build 3D maps of indoor environments. Lai et al. (Lai et al., 2011) also used RGB-D data to recognize instances of a previously trained object. Endres et al. (Endres et al., 2012) used feature descriptors to provide simultaneously the localization and mapping (SLAM) of RGB-D cameras. Their approach was evaluated using SIFT, SURF, and ORB descriptors. We use depth data in background subtraction and also in body part detection. The pixel intensities computed from the RGB values are used for tracking.

The usage of geodesic distances in human body part detection was proposed by Plageman et al. (Plagemann et al., 2010) as part of the Accumulative Geodesic EXtrema points, named the AGEX points. Ganapathi et al. (Ganapathi et al., 2010) used AGEX for performing real time motion capture from depth images. Both studies used depth sensors based on a time-of-flight camera to capture the depth data. AGEX was also used by Baak et al. (Baak et al., 2011) for full body pose reconstruction. Although these studies are very accurate when detecting major body parts (head, hands and feet), the detection of joints in (Plagemann et al., 2010), (Ganapathi et al., 2010), (Baak et al., 2011) is performed as a naïve estimation of their position with respect to the five main body regions, i.e., head, hands and feet. Such an approach might fail when the imaged person is holding objects such as rackets, balls or other video game gadgets. To avoid estimation problems, we use only the positions of each major body part, which are first mapped exactly where the parts are, without any estimation. Considering games, which are the context of our technique, we show that the five main body parts are sufficient for pose classification.

AGEX-points detection is usually performed considering the whole imaged body. In contrast to the conventional approach, we estimate the AGEX points from the pixels of a person's discrete medial axis. We also perform tracking by extracting ASIFT features and matching them between frames. Silberman and Fergus (Silberman and Fergus, 2011) used the SIFT algorithm on depth images for indoor scene segmentation. The main goal of Silberman and Fergus was to label objects (bed, bookshelf, floor, sofa, and table) in a scene, while combining the depth and color images and to obtain satisfactory results. Another study that

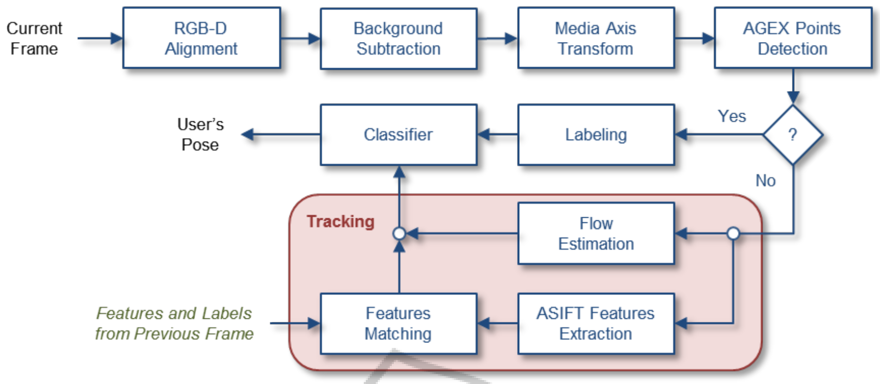

Figure 1: Flowchart of the proposed M5AIE approach applied to RGB-D images to identify the pose of the imaged subject. See Section III for details. The question mark after the AGEX Points Detection stage verifies whether the Labeling stage of the algorithm can be performed.

uses SIFT and depth images was presented by May et al. (May et al., 2008). The main goal in (May et al., 2008) was to perform environment mapping.

3 THE M5AIE METHOD

The M5AIE method aggregates different concepts; some of them were not originally developed for detecting, tracking, and pose classification. The computational flow of the M5AIE algorithm is illustrated in Fig. 1. After the alignment of the RGB (Figure 2a) and depth (Figure 2b) images of a given frame, we use the Minimum Background Subtraction algorithm (Stone and Skubic, 2011) to address most of the unnecessary information in the frame (Subsection 3.1). In turn, the area of the person facing the sensor (Figure 3a) is replaced by the few pixels that define its discrete medial axis (Figure 3b) transformation (Subsection 3.2). The detection of body part candidates begins by building a graph in which each pixel of the medial axis is seen as a vertex that is connected to its neighbors by weighted edges; each weight is given by the Euclidean distance between a pair of pixels (Subsection 3.3). Using this graph, body part candidates are detected through the AGEX points detection method (red points in Figure 3, Subsection 3.4). A labeling step is performed to relate AGEX points to their respective body parts (Subsection 3.5). When labeling fails, the information computed in the previous frame is used in combination with the ASIFT method for tracking the body parts into the current frame (Subsection 3.6). Pose classification is performed in the last stage of our method (Subsection 3.7).

3.1 Minimum Background Subtraction Algorithm

The Minimum Background Subtraction algorithm is composed of training and subtraction stages. During the training stage, the approach limits the background values regarding the following assumptions: indoor environment, static background, and static position and orientation of the sensor. In this stage, a lookup matrix with the same size as the depth image is created to store the minimum depth values assumed by each pixel during a frame sequence that captures only background elements. The subtraction stage is applied to every subsequence frame. By comparing stored minimum values with current depth values, the approach is capable of distinguishing background and foreground pixels (Stone and Skubic, 2011).

Noise is typically present when the Kinect or time-of-flight camera is used. Noise results from errors in the distance measurements, such as when the sensor receives multiple pieces of depth information for the same image coordinates (Schwarz et al., 2012). In the case of the Kinect sensor, one must also address "shadowing". Shadowing occurs when the depth information of the background cannot be captured by the sensor because an object or a person blocks the capturing of this information. Each captured noise pixel and each pixel of the shadow receive a zero value. Because the Minimum Background already provides background values, we apply the same values to every shadow pixel. In this study, we call the output of the Minimum Background algorithm a segmented image. Figure 3a shows a segmented image with the color and depth information aligned.

We chose to use this background subtraction algorithm because it had the best results in previous experiments (Greff et al., 2012).

(a) RGB image

(b) False-color depth information

Figure 2: A pair of images related to the same frame of a sequence: (a) RGB information is used to color the foreground pixels and in the tracking stages of our algorithm. (b) Depth information (displayed with false-color) is used to distinguish background and foreground pixels.

3.2 Discrete Medial Axis Through Distance Transformation

The 2D medial axis transform constitutes finding the centers of the maximum disks that can fit inside of an object (Blum, 1967). A disk is maximal if it is not contained by any other such disk. The set of all centers is called the *medial axis*. When working with digital images, the discrete medial axis of a shape can be computed from the ridge of the discrete distance transformation (Gonzalez and Woods, 2008). Because the discrete medial axis of a discrete object is a connected structure that is composed of a small number of pixels inside that object, we use such a structure to reduce the number of pixels that are to be considered as vertices in the graph computation (Section 3.3).

We have performed discrete medial axis extraction by computing the discrete distance transform of the binary image that results from the Minimum Background Subtraction (Section 3.1). In turn, we have applied mean-C adaptive local thresholding (Gonzalez and Woods, 2008) to identify a superset of the pixels that represent the ridge of the distance transform. From the superset, one could extract the ridge pixels. However, in practice, the exact ridge pixels are not necessary in subsequent steps of our algorithm because the cardinality of the superset is already much smaller than the cardinality of the original set of pixels that represent the users body. A segmented image and the result of the discrete medial axis (superset) extraction through a distance transformation are presented by Figure 3.

3.3 Graph Construction based on Depth Image

We use image pixel coordinates to build a graph in linear time, as implemented in Schwarz et al. (Schwarz et al., 2012). In such a case, two vertices are considered to be neighbors if the corresponding pixels are separated by a maximum distance threshold δ. The graph is represented as $G_t = (V_t, E_t)$, where V_t are the vertices related to pixels in the image plane, and E_t are the edges that connect the vertices. We follow Plagemann et al.'s strategy (Plagemann et al., 2010) to connect two vertices and Schwarz et al.'s scheme to weight the edges with the Euclidean distance of the imaged surface points related to the vertices. Formally, Schwarz et al. define the edges as:

$$E_t = \{(x_{ij}, y_{kl}) \in V_t \times V_t \mid \\ \|x_{ij} - x_{kl}\|_2 < \delta \wedge \|(i,j)^T - (k,l)^T\|_\infty \leq 1\}, \quad (1)$$

where $\|\cdot\|_2$ is the Euclidean distance, $\|\cdot\|_\infty$ is the maximum norm, and $(i,j)^T$ and $(k,l)^T$ are the 2D coordinates of the points x_{ij} and x_{kl} in the depth image. As a consequence of computing the medial axis, the original body can be represented by patches of unconnected pixels. To solve this problem, we used a δ value that connects the disconnected parts. The value of δ was obtained from experiments in which the distance between the unconnected pixels was measured.

3.4 Accumulative Geodesic Extrema Points

Figure 3 illustrates a segmented RGB-D image (Figure 3a), which is used as input to a discrete medial axis transform. Figure 3b illustrates the image from the preprocessing stage that is used to generate the graph. The Accumulative Geodesic Extrema Points (*AGEX*) are selected while considering the distances of the points according to the edges that connect the vertices in the graph G_t (Plagemann et al., 2010). This method maximizes the distances of the points using the Dijkstra algorithm (Dijkstra, 1959). To accomplish this goal, the first AGEX point ($AGEX_1$) is chosen to be the closest point to the centroid (c^t) of the human body. The shortest distance between c^t and all of the other vertices that belong to graph G_t are calculated with Dijkstra's algorithm, and the vertex with the longest distance among all of the shortest distances is selected as $AGEX_2$.

Once the second AGEX point is selected, a zero cost edge between $AGEX_1$ and $AGEX_2$ is added to graph G_t. The aim of adding this edge is to not allow the selection of the same point in a subsequent call of the Dijkstra algorithm. The steps of finding the vertex that has the longest distance in all of the shortest distances that are calculated and adding a zero edge between the two points are repeated considering $AGEX_2$ instead of $AGEX_1$, and so on until $AGEX_6$

can be found. The red points in Figure 3 correspond to the AGEX points of the imaged subject.

Schwarz et al. (Schwarz et al., 2012) approximate the geodesic distances of $AGEX_{k-1}$ and $AGEX_k$ by

$$d_G = \sum_{e \in SP(x,y)} w(e), \tag{2}$$

where $SP(x,y)$ contains all of the edges along the shortest path between the vertices x and y.

3.5 Body Part Labeling

The initialization step for body part labeling comprises a person facing the camera for a few seconds and taking a snapshot on a T-pose (the T-pose can be seen in Figures 2 and 3). The first six AGEX points correspond to the centroid, head, hands and feet, not necessarily selected in that order. They are labeled according to the relative position to the centroid ($AGEX_1$). Until this stage of the process, the hands, feet and head have not been labeled.

Because $AGEX_1$ is the centroid (c^t), we can define the lower and upper parts of the body and separate the other points (from $AGEX_2$ to $AGEX_6$) according to their coordinate values. Assuming the T-pose, the point that has the highest upper value compared with the centroid is considered to be the head. The two points below the centroid are the right and left feet. Finally, the other two points are the right and left hands. These labeled points are considered in the initialization step, and they are detected at the beginning of the image sequence. As long as this configuration remains unchanged, the AGEX method is used to detect and label each of the body parts. However, when the described configuration changes, then we start to use the ASIFT method, using time sequence information that is based on point estimations to track labels from one frame to another, as described in the next subsection.

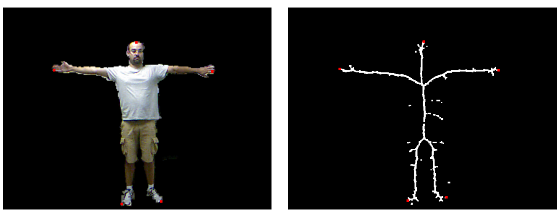

(a) Segmented RGB-D image (b) Input image for graph generation

Figure 3: A discrete medial axis transformation (b) is applied in the segmented RGB-D image (a) to reduce the number of pixels to be considered during the AGEX-graph construction. The red pixels in (a) and (b) are the AGEX points.

3.6 ASIFT-based Tracking of AGEX Points

The ASIFT algorithm was proposed by Morel and Yu (Morel and Yu, 2009) for affine-invariant image-feature extraction. The ASIFT method expects grayscale images as input. The technique transforms the input image by applying tilts and rotations for a small number of latitude angles. Those transformations make ASIFT features affine invariant. Each transformed image is submitted to feature extraction using the SIFT algorithm. See (Morel and Yu, 2009) for more details. The extracted features can be used in image matching applications.

In our tracking strategy, ASIFT is used to identify the features in the frame t that are related to the AGEX points identified in frame $t-1$. However, ASIFT cannot be used directly in tracking due to some practical issues: (i) in the case of background segmented images, ASIFT detects too many features in the border of the foreground region; (ii) there is not necessarily a matching feature for every pixel from one image to another; (iii) the time execution increases as the input images become larger; and (iv) ASIFT can match two features whose positions are far away from an expected conservative maximum distance. We addressed these problems using the following heuristics.

3.6.1 Blurring the Background of Sub-images

With the background pixels colored with black and the RGB color of the body pixels converted to a grayscale, the ASIFT method usually detects features only at the frontier between the foreground and the background regions. To solve this issue, we fill the background pixels of the sub-images with blurred RGB values that are computed according to their colored neighbor pixels. The blurring process makes the sub-images have smoother transitions in intensities among foreground and background pixels. As a result, the contrast inside the portions of the image that are related to the person's body become more significant, which improves the detection of ASIFT features inside the foreground region. Examples of background-blurred sub-images are shown in Figure 5. These examples were computed based on the sub-images in Figure 4. These background-blurred images are the input for the ASIFT, after they are converted to grayscale. The blurring method is performed as follows: The blurring method is performed as follows: The blurring method is performed as follows:

Step 1. Create a list of background pixels and keep it sorted in descending order with regard to the number of foreground (black) 8-connected neighbor pixels of each entry.

Step 2. Replace the RGB value of the first pixel in the list by the mean RGB values of its neighboring foreground pixels. Remove such a pixel from the list, treat it as a foreground pixel and update the order of the remaining pixels.

Step 3. Go to the first step or stop when there is no more background pixel to be processed.

3.6.2 Searching in a Region instead of Searching for Coordinates Only

This heuristic is related to the problem that there is not necessarily a matching feature for every pixel from one image to another. As a consequence of this assumption, a body part position can be lost if we consider only its coordinates. We handle this problem in the following way: if there is no body part matching feature from the sub-image at $t-1$ with the sub-image at t, then we search for the point P, which is the nearest body feature in $t-1$ that has a match in t. We filter the matching result, considering P as the body part and its matching feature in t as the final result.

Considering the person's movement, the body part in frame $t-1$ can be located anywhere in a region of the frame t. The region is delimited according to a distance from the point in $t-1$ and the frame at t. This adaptation is not in ASIFT method but it is in the matching point output. The reference implementation provided by Morel and Yu (Morel and Yu, 2009) returns all matching ASIFT features from an image in $t-1$ and t. Our specialized matching scheme, on the other hand, returns only a single feature in a region in $t-1$ that is related to a feature in t.

3.6.3 Use of Tiny Images instead of Complete Frames

To avoid the heavy computational load of ASIFT applied to the whole image, we apply ASIFT on five tiny images that contain the body parts in frame $t-1$ and the sub-images of the regions in which the same body parts can possibly be found in frame t. It is important to note that the location and labeling of the body parts in frame $t-1$ is always known. In the case of the first frame, the T-pose will guarantee the success of the labeling process. In subsequent frames, the body parts will be found by labeling or tracking processes that are performed in functions of frame $t-2$. Figure 4 illustrates the five sub-images at frame $t-1$. We assume that each body part does not move too much from one frame to the next frame. Each of the tiny images has a different body part in it, which allows the matching features provided by ASIFT to be in approximately the same region from one image to another.

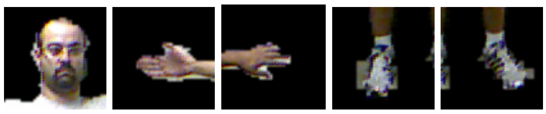

(a) head (b) left hand (c) right hand (d) left foot (e) right foot

Figure 4: Sub-images of the detected five main body parts.

(a) head (b) left hand (c) right hand (d) left foot (e) right foot

Figure 5: Background-blurred version of the sub-images presented in Figure 4.

3.6.4 Body-parts Position Estimation

To assert the consistency of the matching of ASIFT features in the sub-images of consecutive frames, we estimate the expected location of the feature in frame t using the uniform linear motion equation considering its location in frames $t-1$ and $t-2$. The estimation is made using the following:

$$s_t = s_{t-1} + vt, \tag{3}$$

where s_{n-1} is a coordinate value (x or y) of the feature in the previous frame, v is the velocity value calculated from (4), and t is a constant related to time. The velocity value is computed as:

$$v = \frac{\Delta S}{\Delta T}, \tag{4}$$

where ΔT is constant for our case.

The uniform linear motion displacement of each coordinate is computed using:

$$\Delta S = s_{t-2} - s_{t-1}, \tag{5}$$

In our framework, the acquisition of the color and the depth images is performed by the same apparatus (a Kinect), and the RGB-D image alignment is performed by Kinect SDK. However, because of the asynchronous nature of the image sensors, the final aligned RGB-D image could be formed. As a result, background color pixels can be incorrectly mapped to foreground regions. Figure 6 illustrates an extreme case in which many depth pixels of the human body were painted with color information from the background.

To make the proposed matching procedure suitable for tracking, we found four major situations to be addressed, which can be divided into two groups: (i) the matched ASIFT feature and the point estimated with equation (3) correspond to well-mapped background pixels; (ii) the matched ASIFT feature resides in the well-mapped background while the estimated point is part of the users body; (iii) the matched

ASIFT feature belongs to the human body, and the estimated point is part of the background; and (iv) both the matched ASIFT feature and the estimated point correspond to the actual body.

In the first case, our method searches the body part pixel that is closest to the ASIFT feature found. The second case is when the resulting ASIFT feature is part of the background and the estimated point is part of the body, which generates two sub-cases: (a) if the distance between the two points is smaller than a threshold, then the estimated point will be the final result; and (b) if the distance between the two points is larger than a threshold, then the nearest point from the ASIFT feature that belongs to the human body will be the result.

The third case occurs when the ASIFT feature belongs to the human body and the estimated point belongs to the background. In this case, there are two sub-cases, which are similar to the previous case: (i) if the distance between the two points is smaller than the threshold, then the ASIFT matching feature will be the final result; and (ii) if the distance between the two points is larger than the threshold, then the nearest point from the ASIFT feature that belongs to the human body will be the result. Finally, the forth case is when the ASIFT matching feature and the estimated point belong to the human body and, again, we have two sub-cases: (i) if the distance between the two points is smaller than the threshold, then the ASIFT feature is the final result; and (ii) if the distance between the two points is larger than the threshold, then a point whose coordinates are the average of the two points is generated, and this middle point will be the final result.

The four defined heuristics are necessarily because the alignment of the RGB and the depth information could consider images that are acquired at different times. This alignment is provided by the apparatus. If there was no interval for producing RGB-D images, the presented heuristics would be unnecessary.

3.7 Pose Classification

Classification techniques are used in our work to identify categorical labels such as "Pose A" and "Pose B" for the current subject, according to the position of each of the body parts detected or tracked in a given image of the sequence.

We have performed pose classification using three different algorithms: C4.5 Gain Ratio Decision Tree (Quinlan, 1993), the Naïve Bayes classifier (Domingos and Pazzani, 1997) and the KNN Classifier (Cover and Hart, 1967). These algorithms

Figure 6: Kinect performs asynchronous acquisition of RGB and depth images. As a result, the quality of the RGB-D alignment procedure performed by Kinect's API can be affected by rapid movements of the user, which leads to inconsistent RGB-D image formation.

were selected due to their low computational load and simplicity, making them suitable for real-time applications. The main difference between the first two classifiers is that while C4.5 is a decision tree classifier, the Naïve Bayes is based on the Bayes rule of conditional probabilities. In decision trees, attributes are tested, and the final classifications are at the leaves. In this approach, the attributes have a high level of dependency with each other. However, the Naïve Bayes classifier evaluates each attribute individually, considering them to be independent.

In 1967, Cover and Hart (Cover and Hart, 1967) introduced the K-Nearest Neighbor as a pattern classifier. A training set is built by tuples and a tuple X, whose class is unknown, is then tested. The tuple X is compared with each of the training tuples. The K closest tuples to X are considered to predict its class. "Closeness" is considered a distance metric, and it can be calculated, for example, with the Manhattan, Chebyshev or Euclidean distance. The three distances were selected because they use the vertical and horizontal coordinates system, which is used by the M5AIE method to generate tuples. The unknown class of X is assigned to the most common class among its K nearest neighbors.

3.7.1 Bounding Box and Grid

In this work, the algorithms receive as input the labels and the locations of the body parts according to an $N \times N$ grid that is defined inside the bounding box that contains the whole body of the imaged subject. Figure 7 shows the grid squares with $N = 8$. A bounding box was used to identify the cell number of the body parts. The bounding box provides the relative positions according to the detected human body. This approach makes it possible to identify the cell number of the body parts, independently of their occupied positions in the whole segmented image.

All the classification algorithms require the exe-

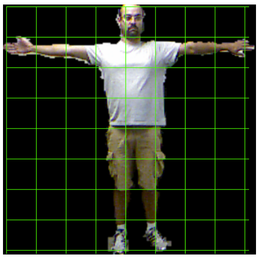

Figure 7: A bounding box limits the human body and it is divided into $N \times N$ cells. In our experiments, $N = 8$.

cution of a training stage to build a model to be used during the classification of the poses. In our work, the dataset used both for training and testing comprises the grid-coordinates that body parts assume at each frame of a set of image sequences produced for this work and the manual classification of the pose in each frame. In the classification procedure, a tuple constitutes a sequence in which the cell position of every individual body part is described in the same order that appears in the attributes definition.

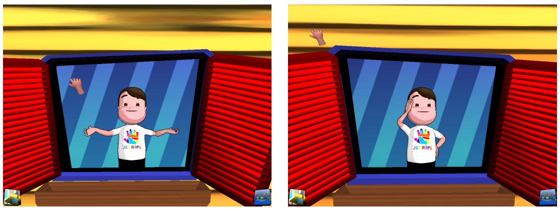

(a) *T-pose* (b) *Dancing*

Figure 8: Illustration of *T-pose* and *dancing* human poses in a game developed by our research group that inspired our experiments.

(a) *Play guitar* (b) *Play flute*

Figure 9: Illustration of *Play guitar* and *Play drums* human poses.

4 EXPERIMENTS AND RESULTS

The described approach was implemented in Python and was evaluated on real image sequences. The ASIFT algorithm was implemented in C++. We used the reference implementation provided by Morel and Yu (Morel and Yu, 2009). We used OpenCV to perform the distance transformation, adaptive thresholding and other basic image processing procedures. The image sequences were collected using a Kinect sensor, which provides both depth and color images with a 640×480 pixel resolution. The resolution of the tiny images was set to 80×80. The goal of this experimental evaluation is to demonstrate the following:

- The modified AGEX can be used for body part detection and labeling in all of the frames of the sequence that have the expected AGEX point configuration described in Section 3;
- The ASIFT algorithm can be used for tracking objectives; and
- The output of the combined techniques can be used for human pose classification.

We previously collected sequences with human poses that were inspired in a game developed by our research group (Brandão et al., 2010). The poses are: *T-pose*, *dancing* (left hand on hip and right hand on head), *playing guitar*, *playing flute* and *playing drums*. Two other movements, which were not related to the game, were also included: *punching* and *kicking*.

Figure 10: Illustration of the *Play drums* human pose.

We characterize the classes as the following: The *T-pose* constitutes a person with both arms and hands at the same level as the shoulders. In the *dancing* class, one of the hands is on the head; the other hand is on the hip, and one or both feet are on the ground. As a consequence, we have six combinations of poses for the class *dancing*: (i) left hand on the head and feet on the ground; (ii) left hand on the head and moving left foot; (iii) left hand on the head and moving right foot; (iv) right hand on the head and feet on the ground; (v) right hand on the head and moving right foot; and (vi) right hand on the head and moving left foot. All of the six poses have the same class, which is *dancing*.

In the *playing guitar* class, the user imitates the moves of playing an instrument, shaking the right hand while the left hand stays at the same level as his/her shoulders. The *playing drums* class is when the user shakes his/her hands up and down alternately. There are two possible poses for the *punch* class, both of which have feet on the ground: (I) right hand and

Table 1: Image sequence evaluation for Volunteer A.

Sequence Number	**Movement**	**Number of Images**	**Track to the end**
Seq. A1	dancing (i)	140	yes
Seq. A2	dancing (i)	116	yes
Seq. A3	dancing (ii)	100	yes
Seq. A4	playing guitar	140	yes*
Seq. A5	playing drums	190	yes*
Seq. A6	playing drums	130	yes*
Seq. A7	playing drums	130	yes*
Seq. A8	punch (I)	84	yes
Seq. A9	punch (I)	81	yes**
Seq. A10	kick (a)	66	yes
Seq. A11	dancing (iii)	58	yes
Seq. A12	dancing (ii)	68	yes
Seq. A13	kick + punch (A)	57	yes
Seq. A14	dancing (iv)	104	yes
Seq. A15	dancing (v)	152	yes
Seq. A16	dancing (vi)	98	yes
Seq. A17	kick + punch (D)	55	yes

*Tracked until the end of the sequence, but there was a problem in the presence of self-occlusion.

**Problem caused by movement velocity.

Table 2: Image sequence evaluation for Volunteer B.

Sequence Number	**Movement**	**Number of Images**	**Track to the end**
Seq. B1	dancing (i)	99	yes
Seq. B2	dancing (iv)	84	yes
Seq. B3	dancing (iii)	84	yes
Seq. B4	dancing (ii)	62	yes
Seq. B5	dancing (v)	72	yes
Seq. B6	dancing (vi)	79	yes
Seq. B7	punch (I)	65	yes
Seq. B8	punch (II)	75	yes
Seq. B9	kick (b)	70	yes
Seq. B10	kick (a)	79	yes
Seq. B11	kick + punch (C)	73	yes
Seq. B12	kick + punch (D)	74	yes
Seq. B13	kick + punch (B)	99	yes
Seq. B14	kick + punch (A)	97	yes

(II) left hand. Similar to the *punch*, the *kick* class can be made with: (a) right foot and (b) left foot, with both hands below the centroid. The *kick + punch* class can be made in four different poses: (A) kick with left foot and punch with left hand; (B) kick with left foot and punch with right hand; (C) kick with right foot and punch with right hand; and (D) kick with right foot and punch with left hand.

We used three different volunteers in our experiments: A, B and C. For each user, we collected a different number of sequences. Volunteer A is male, 1.76 meters tall, and has dark hair. Table 1 shows the collected sequences with Volunteer A. We collected

Table 3: Image sequence evaluation for Volunteer C.

Sequence Number	**Movement**	**Number of Images**	**Track to the end**
Seq. C1	dancing (i)	48	yes
Seq. C2	dancing (iv)	69	yes
Seq. C3	dancing (iii)	45	yes
Seq. C4	dancing (ii)	54	yes
Seq. C5	dancing (v)	54	yes
Seq. C6	dancing (vi)	45	yes
Seq. C7	punch (I)	90	yes
Seq. C8	punch (II)	88	yes
Seq. C9	kick (b)	49	yes
Seq. C10	kick (a)	54	yes
Seq. C11	kick + punch (C)	90	yes
Seq. C12	kick + punch (D)	100	yes
Seq. C13	kick + punch (B)	85	yes

17 sequences with all of the classes.

Volunteer B is male, 1.90 meters tall and has blond hair. Volunteer B made 14 different sequences in four classes, all of them without self-occlusion. All of the possible poses for each of the four classes were collected. Table 2 details each of the collected poses from Volunteer B.

Volunteer C is female, 1.66 meters tall and has dark hair. Similar to Volunteer B, we collected sequences of four different classes with Volunteer C. Additionally, no problem was detected during the collection of the poses, which shows that the M5AIE method works well in sequences that do not have self-occlusions. We collected 13 sequences with Volunteer C because we wanted to test fewer training tuples with the pose *kick + punch* (A).

We observed that the M5AIE method had problems with poses that had self-occlusions. The problems were detected in the *playing guitar* and *playing drums* poses. This problem detection was crucial for the collection of the other users sequences; as a result, we avoided collecting these poses. However, we kept the results to make the tuples and test the classification algorithms. In only one sequence, the tracking method had problems that were caused by the movement velocity, but the pose classification was not affected.

The dataset that was used for both the training and testing comprises the grid-coordinates that body parts assume at each frame of a set of image sequences that were produced for this work and the manual classification of the pose in each frame. In (Brandão et al., 2013), we show how we varied the number of cells of the grid in each frame.

The resume of the experiments of (Brandão et al., 2013) is described as follows: we used three volunteers that had very different biotypes to collect the pose sequences with variations in the numbers of images and poses. In addition to the different classification algorithms, we tested three types of distances: Manhattan, Chebyshev and Euclidean. In all the experiments with the KNN Classifier, as the k value increased, the percentage of correctly classified instances decreased. This happens because if we consider a high number of nearest points, we start to observe very different points that could be far away from the considered point and they affect the final result. We consider KNN with $k = 1$ and the Manhattan distance as the winner because it provided the best results in all of the experiments. We believe that the coordinates of the five main body parts can be normalized in the bounding box because, in our experiments, as long as we increased the division of the used grid (8, 16, 32 and 64), the results became better. However, we also believe that there is a limit when dividing the grid. Further experiments should be performed to find the value for which the division does not make sense anymore. Further experiments should be performed to prove that normalized coordinates could be a good choice in the usage of a bounding box for cell definition.

5 CONCLUSIONS AND FUTURE WORK

We presented the M5AIE method for detecting and tracking five main parts of the human body (head, hands and feet) in sequences of RGB-D images. Our method generates tuples that were used with three different classifiers: the C4.5 Gain Ratio Decision Tree, the Naïve Bayes and the KNN Classifier. The proposed approach combines an effective background subtraction method, the discrete medial axis transformation, in the construction of simpler graphs to be used in the detection of AGEX points, heuristics for labeling, and ASIFT-based tracking of labeled structures.

We investigated how to adapt the ASIFT method for tracking objectives and showed that it is possible to achieve good results with the tested movements. The key insights of this investigation are the following:

- ASIFT and estimation can be combined and used for tracking objectives of movements without self-occlusions;
- It is necessary to make improvements in the tracking method to use it with movements where there is a body part occlusion;
- The RGB-D aligning procedure caused the loss of one of the body parts during tracking. This type of problem might not occur in the future through the synchronous acquisition of color and depth information; and
- The used classifiers are suitable for pose classification purposes.

The three used classifiers worked well. This result shows that the output of the tracking and labeling stages produces qualified tuples that can be used with the adopted classification techniques.

The proposed M5AIE algorithm was implemented in proof-of-concept programs. At this moment, we did not consider the computational load of this specific implementation to be a fundamental requirement because the main goal of this work is to assert the possibility of using a hybrid technique for body part detection, tracking and pose classification. We believe that the M5AIE can be efficiently implemented and used as part of real-time tracking solutions that are applied to games.

The M5AIE method is limited to an indoor environment, static background, static position and orientation of the sensor and to single-user segmentation. Experiments showed that, to be correctly tracked, sequences must not have body part occlusions. Future work will include the application of the M5AIE method with partial occlusion treatment between two users, and the use and comparison of more classifiers for pose recognition with multiple subjects.

REFERENCES

Baak, A., Müller, M., Bharaj, G., Seidel, H.-P., and Theobalt, C. (2011). A data-driven approach for real-time full body pose reconstruction from a depth camera. In *IEEE 13th International Conference on Computer Vision*, pages 1092–1099, Bacelona, Spain.

Blum, H. (1967). A transformation for extracting new descriptors of shape. *Models for the perception of speech and visual form*, 19(5):362–380.

Brandão, A., Brandão, L., Nascimento, G., Moreira, B., Vasconcelos, C. N., and Clua, E. (2010). Jecripe: stimulating cognitive abilities of children with down syndrome in pre-scholar age using a game approach. In *Proceedings of the 7th International Conference on Advances in Computer Entertainment Technology*, ACE '10, pages 15–18, New York, NY, USA. ACM.

Brandão, A., Fernandes, L. A. F., and Clua, E. (2013). A comparative analysis of classification algorithms applied to m5aie-extracted human poses. In *Proceedings of the XII Brazilian Symposium on Games and Digital Entertainment*, SBGAMES '13.

Cover, T. and Hart, P. (1967). Nearest neighbor pattern classification. *Information Theory, IEEE Transactions on*, 13(1):21–27.

Dijkstra, E. (1959). A note on two problems in connexion with graphs. *Numerische Mathematik*, 1(1):269–271.

Domingos, P. and Pazzani, M. (1997). On the optimality of the simple bayesian classifier under zero-one loss. *Machine learning*, 29(2):103–130.

Endres, F., Hess, J., Engelhard, N., Sturm, J., Cremers, D., and Burgard, W. (2012). An evaluation of the rgb-d slam system. In *Robotics and Automation (ICRA), 2012 IEEE International Conference on*, pages 1691–1696.

Ganapathi, V., Plagemann, C., Thrun, S., and Koller, D. (2010). Real time motion capture using a single time-of-flight camera. In *Proceedings of the IEEE Conference on Computer Vision and Pattern Recognition (CVPR)*, pages 755–762, San Francisco, CA, USA.

Gonzalez, R. C. and Woods, R. E. (2008). *Digital Image Processing*. Prentice Hall, 3rd edition.

Greff, K., Brandão, A., Krauß, S., Stricker, D., and Clua, E. (2012). A comparison between background subtraction algorithms using a consumer depth camera. In *Proceedings of International Conference on Computer Vision Theory and Applications - VISAPP*, volume 1, pages 431–436, Rome, Italy. SciTePress.

Henry, P., Krainin, M., Herbst, E., Ren, X., and Fox, D. (2012). Rgb-d mapping: Using kinect-style depth cameras for dense 3d modeling of indoor environments. *The International Journal of Robotics Research*, 31(5):647–663.

Lai, K., Bo, L., Ren, X., and Fox, D. (2011). Sparse distance learning for object recognition combining rgb and depth information. In *IEEE International Conference on on Robotics and Automation*.

May, S., Droeschel, D., Holz, D., Wiesen, C., and Fuchs, S. (2008). 3d pose estimation and mapping with time-of-flight cameras. In *IEEE/RSJ International Conference on Intelligent Robots and Systems (IROS), Workshop on 3D Mapping*, pages 1–6, Nice, France.

Morel, J.-M. and Yu, G. (2009). Asift: A new framework for fully affine invariant image comparison. *SIAM J. Img. Sci.*, 2(2):438–469.

Mota, V., Perez, E., Vieira, M., Maciel, L., Precioso, F., and Gosselin, P. (2012). A tensor based on optical flow for global description of motion in videos. In *Graphics, Patterns and Images (SIBGRAPI), 2012 25th SIBGRAPI Conference on*, pages 298–301.

Plagemann, C., Ganapathi, V., Koller, D., and Thrun, S. (2010). Real-time identification and localization of body parts from depth images. In *Proceedings of the IEEE International Conference on Robotics & Automation (ICRA)*, pages 3108–3113, Anchorage, Alaska, USA.

Quinlan, J. R. (1993). *C4.5: programs for machine learning*. Morgan Kaufmann Publishers Inc., San Francisco, CA, USA.

Schwarz, L. A., Mkhitaryan, A., Mateus, D., and Navab, N. (2012). Human skeleton tracking from depth data using geodesic distances and optical flow. *Image Vision Comput.*, 30(3):217–226.

Shotton, J., Fitzgibbon, A., Cook, M., Sharp, T., Finocchio, M., Moore, R., Kipman, A., and Blake, A. (2011). Real-time human pose recognition in parts from single depth images. In *Proceedings of the IEEE Conference on Computer Vision and Pattern Recognition (CVPR)*, pages 1297–1304, Colorado Springs, CO, USA.

Silberman, N. and Fergus, R. (2011). Indoor scene segmentation using a structured light sensor. In *Proceedings of the International Conference on Computer Vision - Workshop on 3D Representation and Recognition*, pages 601–608.

Stone, E. and Skubic, M. (2011). Evaluation of an inexpensive depth camera for passive in-home fall risk assessment. In *5th International Conference on Pervasive Computing Technologies for Healthcare (PervasiveHealth), 2011*, pages 71 –77.

Ye, M., Wang, X., Yang, R., Ren, L., and Pollefeys, M. (2011). Accurate 3d pose estimation from a single depth image. In *Proceedings of International Conference on Computer Vision*, pages 731–738. IEEE.